Carlo Pierpaoli, MD • Peter Jezzard, PhD • Peter J. Basser, PhD • Alan Barnett, PhD
Giovanni Di Chiro, MD

Diffusion Tensor MR Imaging of the Human Brain[1]

PURPOSE: **To assess intrinsic properties of water diffusion in normal human brain by using quantitative parameters derived from the diffusion tensor, D, which are insensitive to patient orientation.**

MATERIALS AND METHODS: **Maps of the principal diffusivities of D, of Trace(D), and of diffusion anisotropy indices were calculated in eight healthy adults from 31 multisection, interleaved echo-planar diffusion-weighted images acquired in about 25 minutes.**

RESULTS: **No statistically significant differences in Trace(D) ($\approx$2,100 $\times$ 10^{-6} mm^2/sec) were found within normal brain parenchyma, except in the cortex, where Trace(D) was higher. Diffusion anisotropy varied widely among different white matter regions, reflecting differences in fiber-tract architecture. In the corpus callosum and pyramidal tracts, the ratio of parallel to perpendicular diffusivities was approximately threefold higher than previously reported, and diffusion appeared cylindrically symmetric. However, in other white matter regions, particularly in the centrum semiovale, diffusion anisotropy was low, and cylindrical symmetry was not observed. Maps of parameters derived from D were also used to segment tissues based on their diffusion properties.**

CONCLUSION: **A quantitative characterization of water diffusion in anisotropic, heterogeneously oriented tissues is clinically feasible. This should improve the neuroradiologic assessment of a variety of gray and white matter disorders.**

DIFFUSION-WEIGHTED (DW) images are magnetic resonance (MR) images with signal intensities sensitized to the random motion of water molecules (1–3). This is usually achieved by including strong magnetic field gradient pulses in the imaging sequence. From a series of DW images, it is possible to calculate an apparent diffusion coefficient (ADC) of water molecules in the direction of the diffusion sensitizing gradient (2).

A number of studies have suggested that images of water diffusivity can provide information about tissue pathophysiology complementary to that contained in T1- and T2-weighted images (4). The most clinically important results to date pertain to the assessment of brain diseases, especially acute cerebral ischemia (5), where a significant reduction in the ADC of water demarcates the ischemic regions before signal intensity changes are detectable in conventional T2-weighted images (6).

Although the determinants of water diffusion in tissues are still not completely understood, there is general agreement that physicochemical properties of the tissue (eg, viscosity and temperature) as well as its structural components (macromolecules, membranes, and intracellular organelles) can substantially affect water diffusivity. Their importance in determining the behavior of water diffusivity is suggested by the observation that in tissues that have a random microstructure, the measured ADC appears to be the same in all directions (isotropic diffusion), while in tissues that have a regularly ordered microstructure, the measured ADC varies with tissue orientation (anisotropic diffusion). This phenomenon has been observed in white matter (7–9); in skeletal (10), cardiac (11), and uterine (12) muscles; in portions of the kidney (13); and in the lens (14). It is reasonable to speculate that pathologic conditions that alter tissue microstructure could affect not only the bulk diffusivity, but also the anisotropic diffusion characteristics of water or metabolites.

Assessing diffusion in anisotropic tissues, however, requires a knowledge of molecular displacements in all directions, whereas the ADC only provides a measure of the displacements of molecules in one direction. Efforts to characterize anisotropic diffusion by measuring ADCs in two or three perpendicular directions have been made (15–18). Implicit in these schemes are the assumptions that the larger ADC represents the diffusion coefficient parallel to the longitudinal axis of the anisotropic structure and

Index terms: Brain, MR, 13.121412, 13.121416, 13.12146 • Magnetic resonance (MR), diffusion study, 13.121412, 13.121416, 13.12146, 13.92 • Magnetic resonance (MR), experimental, 13.121412, 13.121416, 13.12146, 13.92 • Magnetic resonance (MR), tissue characterization, 13.121412, 13.121416, 13.12146, 13.92

Abbreviations: ADC = apparent diffusion coefficient, CSF = cerebrospinal fluid, DW = diffusion weighted, ROI = region of interest, S/N = signal-to-noise ratio, TE = echo time.

Radiology 1996; 201:637–648

[1] From the Neuroimaging Branch, National Institute of Neurological Diseases and Stroke (C.P., A.B., G.D.C.); Unit of MRI Physics, National Institute of Mental Health (P.J.); and the National Center for Research Resources (P.J.B.); National Institutes of Health, Bldg 10, Room 1C227, 9000 Rockville Pike, Bethesda, MD 20892-1178. Received July 3, 1996; revision requested August 12; revision received August 19; accepted August 26. **Address reprint requests to** C.P.

that the smaller ADC is a measure of water diffusivity perpendicular to it.

Unfortunately, these conditions are impossible to satisfy in clinical MR imaging of heterogeneously oriented tissues, such as brain white matter, because it is not possible to align the diffusion gradients with the axes of the fibers in all voxels. The dependence of the ADC on gradient direction introduces an orientation bias into anisotropy indices which can lead to erroneous conclusions about tissue structure and potentially to diagnostic errors. For example, it has been recently demonstrated in monkey brain that various measures of diffusion anisotropy using ADCs acquired with diffusion gradients applied in three perpendicular directions, ADC_x, ADC_y, and ADC_z, generally underestimate the degree of diffusion anisotropy of white matter structures (19). The error is so severe in white matter fibers oriented obliquely with respect to the magnet coordinates as to make these fibers appear isotropic, indistinguishable from gray matter.

Moreover, implicit in the use of the ratio of ADCs as an anisotropy measure is the assumption of cylindrical symmetry of the tissue, that is, that there are only two relevant directions, one that is parallel and the other that is perpendicular to the fiber tract. This view of fiber architecture, while probably appropriate for some tissue structures, is generally too simplistic.

The estimation of a diffusion tensor, **D**, has been proposed as an effective means to overcome these problems of characterizing diffusion in anisotropic, heterogeneously oriented tissues (20,21). The six independent scalar elements of the diffusion tensor contain the information required to characterize diffusion in all directions. Moreover, by using them, it is possible to calculate new quantities that are intrinsic to the tissue, that is, that are rotationally invariant, independent of the orientation of the subject in the magnet.

The most fundamental rotationally invariant quantities are the three principal diffusivities (eigenvalues) of **D**, which are the principal diffusion coefficients measured along the three (intrinsic) coordinate directions that constitute the local fiber frame of reference in each voxel. (Each eigenvalue is associated with a principal direction [eigenvector] that is also intrinsic to the tissue. The three eigenvectors of **D** are mutually perpendicular and define the local "fiber" frame of reference in which the description of diffusion is the simplest and most natural.) In each voxel, these eigenvalues can be sorted in order of decreasing magnitude (λ_1 = highest diffusivity, λ_2 = intermediate diffusivity, and λ_3 = lowest diffusivity). In anisotropic tissues organized in parallel bundles, the largest eigenvalue, λ_1, represents the diffusion coefficient along the direction parallel to the fibers ($ADC_\parallel$), while λ_2 and λ_3 represent the transverse diffusion coefficients ($ADC_\perp$ and $ADC_\perp'$).

Finally, from **D** one can compute scalar measures that characterize specific features of the diffusion process, such as Trace(**D**) that is used to measure the orientationally averaged diffusivity and quantities that are used to measure the degree of diffusion anisotropy. More general information about the underpinnings of diffusion tensor MR imaging may be found in recent review articles (22).

We performed this study to characterize the diffusion properties of water in the human brain by using the principal diffusivities or eigenvalues of **D**, along with Trace(**D**) and diffusion anisotropy indices derived from **D**. These measures share the attributes of being quantitative and independent of the position and orientation of the subject within the magnet. We also considered the technical requirements for measuring the diffusion tensor in a clinical setting.

MATERIALS AND METHODS

Subjects

Eight adult healthy volunteers (aged 27–36 years) participated in the study under a protocol approved by the Institutional Review Board of the National Institute of Neurological Diseases and Stroke (Bethesda, Md). Written informed consent was obtained before each study. Each subject underwent MR imaging at least once to acquire a data set of axial DW images; four of the eight subjects also underwent imaging to obtain sagittal, coronal, or both sagittal and coronal data sets.

MR Imaging

Studies were performed with a 1.5-T magnet (Signa Advantage; GE Medical Systems, Milwaukee, Wis) equipped with a gradient insert (Medical Advances, Milwaukee, Wis) capable of producing gradient pulses up to 25 mT/m and a birdcage quadrature radio-frequency coil. Reduction of subject head motion was achieved by gently inflating two custom-built pneumatic pillows placed on either side of the subject's head. After positioning the subject with the help of gradient-recalled-echo sagittal and axial images, the magnetic field was shimmed by using the standard nonlocalized shimming routine provided by the manufacturer.

Diffusion images were acquired with a recently developed interleaved spin-echo, echo-planar imaging sequence (23) with a navigator echo used to correct for motion artifacts (24–28). The navigator-echo correction was accomplished by collecting a read-direction navigator echo as part of the data acquisition of each echo-planar interleaf. An additional "reference" image was used to correct for ghosting due to the odd and even echoes of the echo-planar readout. A description of the pulse sequence diagram and the algorithm for image reconstruction is presented elsewhere (23).

Diffusion sensitization was attained by applying identical trapezoidal diffusion gradient pulses before and after the 180° radio-frequency pulse (29). These gradients had a duration of 22 msec and a ramp time of 0.2 msec and were separated by a time interval of 42.4 msec (center to center). To attain the maximum diffusion sensitization for a given echo time (TE), the diffusion gradients were asymmetrically positioned with respect to the 180° radio-frequency pulse. Six different gradient directions were sampled sequentially by applying pairs of diffusion gradients, G_x, G_y, and G_z, simultaneously. The following directional pattern was used for the six gradients: $\{(1/G_0)(G_x, G_y, G_z) = (1,0,1), (-1,0,1), (0,1,1), (0,1,-1), (1,1,0), (-1,1,0)\}$, where (for the acquisition of axial images) G_x is the component of the diffusion gradient in the phase-encoding direction (horizontal), G_y is the component of the diffusion gradient in the readout direction (vertical), G_z is the component of the diffusion gradient in the section-select direction (bore), and G_0 is the strength of the diffusion gradient.

In each direction, we acquired five DW images with different diffusion gradient strengths. The maximum gradient strength was 23 mT/m. A total of 31 DW images were obtained for each section, which included one image obtained with no diffusion sensitization. The values of the Trace of the b-matrix ranged between 0.2 sec/mm^2 and 1,016 sec/mm^2.

Imaging acquisition parameters were as follows: 18 axial sections, 3-mm section thickness, 2-mm section separation, 128 × 128 in-plane resolution (eight interleaves, 16 echoes per interleaf), 220-mm field of view, a repetition time of greater than 5 seconds and a TE of 80 msec, and cardiac gating (two to three acquisitions per heartbeat, depending on the heart rate, starting with a 200-msec delay after systole).

The imaging time for the acquisition of the entire diffusion imaging data set was usually less than 25 minutes (24.8 minutes, assuming a heart rate of 60 beats per minute). Including positioning and shimming, the total time spent in the magnet by the subject was about 40 minutes.

Analysis of the MR Imaging Data

The raw data were transferred to a Sparc-10 workstation (Sun Microsystems,

Mountain View, Calif) and processed for phase correction, navigator-echo correction, and Fourier reconstruction. For each reconstructed magnitude image, the b-matrix (30) was numerically calculated from the imaging and gradient waveforms. The six independent elements of the diffusion tensor **D** (D_{xx}, D_{yy}, D_{zz}, D_{xy}, D_{xz}, D_{yz}) and the signal intensity without diffusion sensitization, A(**b** = **0**), were statistically estimated in each voxel according to the method of Basser et al (20,21).

Background noise levels were measured in regions of the images that contained no tissue (31). These regions were chosen in the frequency-encoding direction to avoid contamination by signals originating from ghosts present in the phase-encoding direction. A mask was then applied to exclude all voxels having a non–diffusion-weighted signal intensity of less than eight times the average background noise level. The square of the deviation between each measured value of the logarithm of signal magnitude and the corresponding value predicted by the model (which appears as a term in χ^2) was normalized by the square of the ratio of the root-mean-squared background noise in each image and the signal intensity in each voxel. This properly weights the observed deviation in each measurement by the experimental variance corrected for the bias introduced by taking the logarithm of the signal intensity (32).

Once **D** was calculated in each voxel, its eigenvectors and eigenvalues were obtained by using the numeric routine TQLI (33) provided in IDL (Iterative Data Language; Research Systems, Boulder, Colo). The eigenvalues of **D** were then sorted in order of decreasing magnitude in each voxel.

Maps of rotationally invariant parameters derived from **D**, including the Trace of the diffusion tensor, Trace(**D**), and two recently proposed anisotropy indices, the *Volume Ratio* index (19,34) and the *Lattice* anisotropy index (19,35), were also calculated on a voxel-by-voxel basis directly from the map of **D**. The Volume Ratio is an *intravoxel* anisotropy index that represents geometrically the ratio of the volume of an ellipsoid whose semimajor axes are the three eigenvalues of **D** and the volume of a sphere whose radius is the mean diffusivity, Trace(**D**)/3. The Lattice anisotropy index is an *intervoxel* measure of diffusion anisotropy that exploits information about the orientational coherence of the eigenvectors of **D** in adjacent voxels to improve the estimate of diffusion anisotropy within a reference voxel. The *Lattice* anisotropy index is especially immune to background noise in the DW images and provides a quantitative, robust measurement of diffusion anisotropy (19,35).

Averages of these imaging parameters were also obtained in different regions of interest (ROIs) by adding their values on a voxel-by-voxel basis. Anatomic ROIs were drawn by a trained neurologist (C.P.) on the T2-weighted axial amplitude images of A(**b**=**0**). ROIs of small anatomic structures on the in-plane images were constructed by pooling voxels of the same structures in different sections.

Statistical Analysis of the Data

After estimating **D** in each voxel, the correlation coefficient (calculated in each voxel during the regression procedure) was used to mask or exclude voxels in which the linear model poorly fit the data. Voxels with a correlation coefficient of less than 0.85 were excluded from further consideration. To assess the statistical significance of variations of Trace(**D**) and the anisotropy indices between different anatomic regions, we used one-way analysis of variance followed by post hoc comparisons with the Sheffe test.

In principle, if there were no noise in DW imaging, one could determine whether water diffusion is isotropic ($\lambda_1 = \lambda_2 = \lambda_3$), cylindrically symmetric and anisotropic ($\lambda_1 \neq \lambda_2 = \lambda_3$, or $\lambda_1 = \lambda_2 \neq \lambda_3$), or asymmetric and anisotropic ($\lambda_1 \neq \lambda_2 \neq \lambda_3$) in each anatomic ROI by inspecting the eigenvalues. However, when the DW images are noisy, sorting the eigenvalues biases their distributions (19), so that standard statistical tests that analyze the significance of their differences are not valid.

To address this problem, we have used an empiric hypothesis-testing procedure instead. To test the hypothesis of diffusion isotropy in each ROI, we constructed an isotropic diffusion tensor whose Trace equaled the experimentally measured Trace(**D**) in the ROI. Distributions of the three eigenvalues of **D** were then generated by using Monte Carlo simulations (19). In these simulations, the signal-to-noise ratio (S/N) was identical to that measured in each ROI. It was obtained by dividing the mean signal intensity in the ROI by the root-mean-squared background noise (31). Moreover, the b-matrices were the same as those used in the present study. We used a one-tailed *t* test with λ_1 and λ_3 and a two-tailed *t* test with λ_2 to assess whether there were significant differences between actual (measured) and expected (simulated) distributions of each eigenvalue.

If significant differences were assessed in at least one of the eigenvalues, the hypothesis of isotropic diffusion in the ROI was rejected. In such ROIs, the hypothesis of cylindrically symmetric and anisotropic diffusion was then tested in turn. This was done by generating a set of diffusion tensors whose Trace equaled the ROI-averaged Trace(**D**) but for which $\lambda_1 \neq \lambda_2 = \lambda_3$ or $\lambda_1 = \lambda_2 \neq \lambda_3$. Monte Carlo simulations were then performed (as described above) by using these cylindrically symmetric tensors. We selected tensors whose mean values of λ_1 and λ_3 matched those measured in the ROI. Then, by using a one-tailed *t* test, we were able to assess whether significant differences existed between actual (measured) and expected (simulated) distributions of λ_2. If such differences were not significant, we concluded that the tissue was cylindrically symmetric and anisotropic; otherwise, we concluded that the tissue was asymmetric and anisotropic.

RESULTS

The head restraint was well tolerated by all subjects, and all subjects completed the study. The use of head restraint and cardiac gating did not entirely eliminate motion artifacts in DW images, so a navigator-echo–correction scheme was necessary to obtain usable data. Overall, about 10% of the DW images were corrupted by motion artifacts even after navigator-echo correction. The S/N of the non–DW images was relatively constant in the various studies: about 18–20 in white matter, 22 in deep gray matter, and 25 in cortical gray matter. By means of direct computation, the contribution of the imaging gradients to the b-matrix was found to be negligible (less than 1%) for all the images.

Diagonal and Off-diagonal Elements of D

For an axial section of the brain, Figure 1a shows images of the diagonal elements of **D** (D_{xx}, D_{yy}, and D_{zz}), which correspond to the ADCs in the x, y, and z directions, respectively. (We did not measure the ADCs along the x, y, and z coordinate directions directly because we applied diffusion sensitizing gradients only along oblique directions. When imaging gradients can be shown to have a negligible effect on echo attenuation, ADC_x, ADC_y, and ADC_z are equal to the corresponding diagonal elements of the diffusion tensor.) Figure 1b shows images of the off-diagonal elements of **D** (D_{xy}, D_{xz}, and D_{yz}). Both the diagonal and off-diagonal elements of **D** depend on the intrinsic diffusion properties and the orientation of the tissue; however, the off-diagonal elements of **D** do not represent ADCs along the oblique directions. Rather, they indicate how strongly random displacements are correlated in the x, y, and z directions. The gray background of the images in Figure 1b corresponds to a zero value, which indicates no correlation; brighter voxels indicate a positive correlation; and darker voxels indicate a negative correlation. When all off-diagonal elements are zero, it may indicate isotropy or that locally fibers lie parallel to the x, y, or z axes. In both cases, the estimation of the entire diffusion tensor would not be necessary to properly characterize anisotropy, and ADCs measured along the three magnet axes would be sufficient.

Positive or negative values of the off-diagonal elements of **D** indicate regions where the anisotropic struc-

tures are oblique with respect to the x, y, or z axes. In this case, one would underestimate the degree of anisotropy by using ADC_x, ADC_y, and ADC_z rather than the eigenvalues of **D**. As we can see in Figure 1b, a number of regions in the corpus callosum, centrum semiovale, and subcortical white matter possess off-diagonal elements that are nonzero.

In Figure 1b, notice that all voxels at the periphery of the brain have nonzero off-diagonal elements. This is surprising because these regions contain cerebrospinal fluid (CSF), and therefore should exhibit no anisotropic diffusion. This finding is artifactual. It is due to shearing and dilatational distortion of the DW images caused by eddy currents induced when diffusion gradients are applied. The misregistration of the distorted DW images introduces an artifact in the estimation of **D**. This results in blurring of maps of quantities derived from **D** and the appearance of spurious boundaries—regions of apparently increased anisotropy—at the interfaces between structures having markedly different diffusion properties.

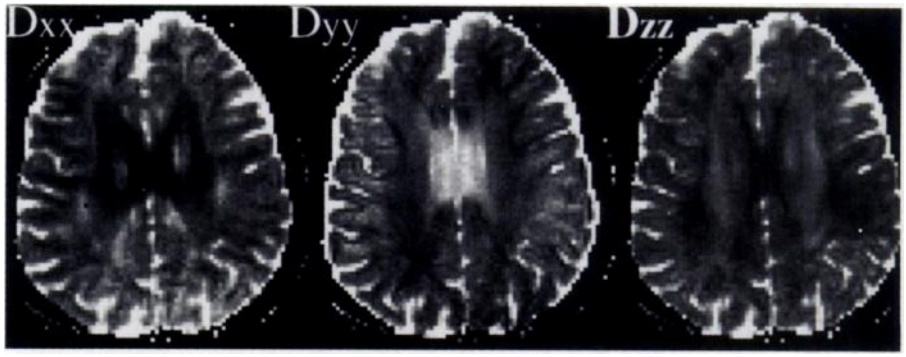

a.

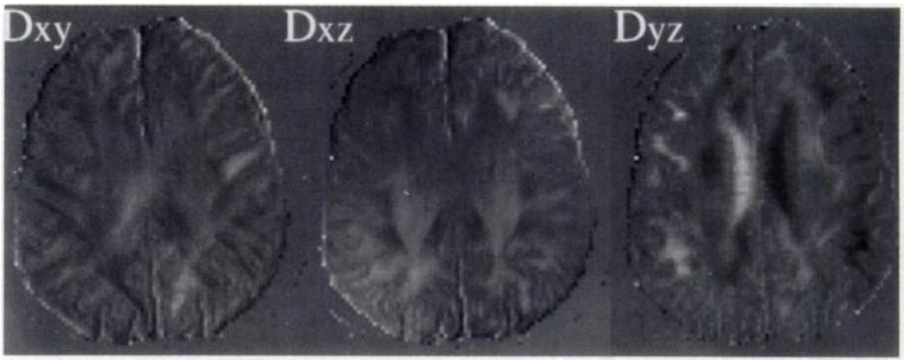

b.

Figure 1. Axial maps of diffusion tensor elements in the brain of a healthy 33-year-old woman. **(a)** Images of the diagonal elements of **D**: D_{xx}, D_{yy}, and D_{zz}, which correspond to ADC_x, ADC_y, and ADC_z, respectively. Black corresponds to 0 mm^2/sec and white corresponds to 2,500 × 10^{-6} mm^2/sec. **(b)** Images of the off-diagonal elements of **D**: D_{xy}, D_{xz}, and D_{yz}. Gray-scale values lie between −1,250 × 10^{-6} mm^2/sec and 1,250 × 10^{-6} mm^2/sec. Image contrast of all elements of **D** depends on both the intrinsic diffusion properties of the tissue and the orientation of the subject in the magnet.

Eigenvalues of D

Figure 2 comprises maps of the three sorted eigenvalues of **D** (λ_1, λ_2, and λ_3), computed from the six images depicted in Figure 1. The eigenvalues of **D** are the three principal diffusion coefficients that are characteristics of the tissue, so that, unlike ADC_x, ADC_y, and ADC_z, they do not depend on the direction along which the diffusion gradients have been applied. We see that, in contrast with the images of the elements of **D** in Figure 1, we do not detect any orientational bias in the images in Figure 2. The image of λ_1, for example, is a map of the highest diffusion coefficient measurable in each voxel, while the image of λ_3 is a map of the smallest diffusion coefficient measurable in each voxel for all possible directions of diffusion sensitizing gradients. In gray matter, it can be seen that the images of λ_1, λ_2, and λ_3 show similar, but not equal, intensities. This is also the case in regions of CSF. Anisotropic structures, such as white matter, exhibit marked differences in intensity in the three different images.

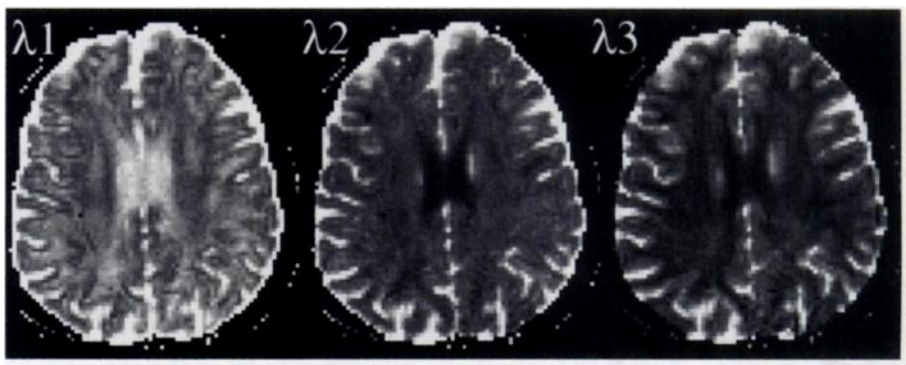

Figure 2. Maps of the three sorted eigenvalues of **D** (λ_1, λ_2, and λ_3) computed from the maps of the six diagonal elements of **D** depicted in Figure 1. Structures in which diffusion is isotropic should have the same intensity in the three images, while structures that are anisotropic should exhibit significant differences in intensity in the three different images. If the two diffusion coefficients perpendicular to the fiber tracts were the same (cylindrically symmetric and anisotropic diffusion), we would also expect the contrast in the images of λ_2 and λ_3 to be the same. For most white matter regions, this condition is not satisfied.

Table 1 contains the eigenvalues of **D** (λ_1, λ_2, and λ_3) juxtaposed with the diagonal elements of **D** measured in different anatomic ROIs in the brain. Average values of Trace(**D**) and of the Volume Ratio and the Lattice anisotropy indices in these ROIs are also presented. Table 2 summarizes our analysis of the anatomic ROIs presented in Table 1. Trace(**D**) is approximately 2,100 × 10^{-6} mm^2/sec in most brain regions but is approximately 2,400 × 10^{-6} mm^2/sec in the cortex. Table 2 shows that no statistically significant differences exist between Trace(**D**) in different ROIs, with the exception of in the cortex, where the value is significantly higher than it is in all the other regions.

The sorted eigenvalues of **D** suggest that water diffusion is highly anisotropic in some white matter structures, such as in the pyramidal tract and in the corpus callosum, where the values of λ_1 ($\approx$ 1,700 × 10^{-6} mm^2/sec) are much larger than the values of λ_2 ($\approx$ 300 × 10^{-6} mm^2/sec) and λ_3 ($\approx$ 110 ×

Table 1
Eigenvalues and Diagonal Elements of D, Trace (D), and Two Anisotropy Measures Obtained in Nine ROIs

Measure	Pyramidal Tract	Splenium of the Corpus Callosum	Optic Radiation	Posterior Limb of the Internal Capsule	U Fibers	Centrum Semiovale	Caudate Nucleus	Frontal Cortex	Cerebrospinal Fluid
Eigenvalues of **D** ($\times 10^{-6}$ mm²/sec)									
λ_1	1,708 ± 131	1,685 ± 121	1,460 ± 75	1,320 ± 54	1,200 ± 79	995 ± 66	783 ± 55	1,002 ± 118	3,600 ± 235
λ_2	303 ± 71	287 ± 71	496 ± 59	447 ± 36	545 ± 64	602 ± 32	655 ± 28	810 ± 65	3,141 ± 144
λ_3	114 ± 12	109 ± 26	213 ± 67	139 ± 41	208 ± 73	349 ± 17	558 ± 17	666 ± 53	2,932 ± 212
Diagonal elements of **D** ($\times 10^{-6}$ mm²/sec)									
D_{XX}	311 ± 131	841 ± 486	933 ± 507	451 ± 99	455 ± 138	606 ± 119	635 ± 69	874 ± 102	3,187 ± 165
D_{YY}	420 ± 188	942 ± 537	827 ± 490	380 ± 84	456 ± 176	603 ± 103	706 ± 91	795 ± 136	3,080 ± 178
D_{ZZ}	1,340 ± 245	287 ± 143	405 ± 62	1,070 ± 98	1,040 ± 84	736 ± 93	656 ± 35	809 ± 36	3,206 ± 162
Trace (**D**) ($\times 10^{-6}$ mm²/sec)	2,125 ± 132	2,081 ± 141	2,169 ± 77	1,906 ± 80	1,953 ± 154	1,945 ± 73	1,996 ± 52	2,477 ± 164	9,573 ± 305
Anisotropy measures									
1 − volume ratio	0.93 ± 0.04	0.86 ± 0.05	0.62 ± 0.12	0.70 ± 0.08	0.55 ± 0.11	0.27 ± 0.03	0.08 ± 0.03	0.08 ± 0.05	0.02 ± 0.01
Lattice index	0.73 ± 0.06	0.77 ± 0.05	0.54 ± 0.07	0.61 ± 0.04	0.46 ± 0.05	0.31 ± 0.03	0.12 ± 0.05	0.09 ± 0.04	0.05 ± 0.02

Note.—Values are expressed as mean ± standard deviation.

Table 2
Statistical Analysis of Diffusion Anisotropy and Trace (D) between ROIs

	ROI							
ROI	Frontal Cortex	Caudate Nucleus	Centrum Semiovale	U Fibers	Optic Radiation	Internal Capsule	Pyramidal Tract	Corpus Callosum
Lattice anisotropy index								
Frontal cortex	...	No	Yes	Yes	Yes	Yes	Yes	Yes
Caudate nucleus	No	...	Yes	Yes	Yes	Yes	Yes	Yes
Centrum semiovale	Yes	Yes	...	Yes	Yes	Yes	Yes	Yes
U fibers	Yes	Yes	Yes	...	No	Yes	Yes	Yes
Optic radiation	Yes	Yes	Yes	No	...	No	Yes	Yes
Internal capsule	Yes	Yes	Yes	Yes	No	...	No	Yes
Pyramidal tract	Yes	Yes	Yes	Yes	Yes	No	...	No
Corpus callosum	Yes	Yes	Yes	Yes	Yes	Yes	No	...
Trace (**D**)								
Frontal cortex	...	Yes	Yes	Yes	Yes	Yes	Yes	Yes
Caudate nucleus	Yes	...	No	No	No	No	No	No
Centrum semiovale	Yes	No	...	No	No	No	No	No
U fibers	Yes	No	No	...	No	No	No	No
Optic radiation	Yes	No	No	No	...	No	No	No
Internal capsule	Yes	No	No	No	No	...	No	No
Pyramidal tract	Yes	No	No	No	No	No	...	No
Corpus callosum	Yes	No	No	No	No	No	No	...

Note.—$P < .05$ indicated a statistically significant difference. "Yes" indicates significance and "no" indicates no significance at the $P < .05$ level by using the Sheffe test.

10^{-6} mm²/sec). The pyramidal tract and the corpus callosum also have the highest values of the 1 − Volume Ratio and Lattice anisotropy indices. The degree of anisotropy is substantially lower in other white matter regions, with the lowest values observed in the centrum semiovale. In contrast with the results obtained for Trace(**D**), the Volume Ratio and Lattice anisotropy indices show significant differences among many white matter regions (Table 2).

In all regions, the diagonal elements of **D** in the x, y, and z directions (which in this study are equivalent to ADCs in the x, y, and z directions) are significantly different from the eigenvalues of **D**. Within each ROI, the range of values of the ADCs is always lower than the range of the eigenvalues of **D**. These differences, however, are more pronounced in some anatomic regions than in others and depend primarily on the degree of misalignment of the fiber tract axis with respect to the magnet x, y, and z coordinates.

Moreover, in regions that contain anisotropic structures, the ADCs in the x, y, and z directions exhibit significantly higher intersubject variability (as reflected in the standard deviation) than the eigenvalues of **D**. Higher intersubject variability of the ADCs is due to their dependence on the orientation of the anisotropic structures. This artifact is removed by comparing the eigenvalues, which are intrinsic to the tissue and independent of its orientation.

Clustering and Classifying Tissue on the Basis of Diffusion Properties

Another advantage of working with measures of diffusion that are not affected by fiber orientation is that they can be used as features with which to cluster and classify tissues. Figure 3 is a scatter plot that displays values of the 1 − Volume Ratio anisotropy index and the Trace(**D**) in each voxel of an axial brain section as x-y coordinate pairs. Voxels with low values of anisotropy and Trace(**D**) correspond mainly to regions of gray

matter, voxels with high anisotropy but low Trace(**D**) correspond mainly to regions of white matter, and voxels with low anisotropy and high Trace(**D**) correspond to regions of CSF.

Such classification is impossible when only the ADCs are used. In the scatter plot, however, the clusters that correspond to gray matter, white matter, and CSF regions are not disjoint (well demarcated). This is caused in part by partial volume contamination, because some voxels may contain a mixture of tissue types. This artifact is especially likely to manifest itself in voxels at the boundary between cortical gray matter and CSF. Another reason why we do not see distinct clusters is that, unlike Trace(**D**), the degree of anisotropy varies markedly among different white matter regions. While the anisotropy in the corpus callosum or the pyramidal tract is clearly higher than that in gray matter, the anisotropy in other white matter regions may be so low that they could be misclassified as gray matter. Within a large ROI that contains white matter regions, one sees a continuum in the degree of diffusion anisotropy.

Figures 4, 5, and 6 are a series of axial, coronal, and sagittal images, respectively. The top rows of each figure show images of A(**b**=**0**), which is a T2-weighted image with the same contrast as a non–DW image but that has less background noise because it is derived from the entire set of 31 DW images (as described above). The second row of each of the figures shows the Lattice anisotropy index images. Regions of highly ordered white matter fiber tracts appear hyperintense on these images, whereas isotropic regions appear black. The greatest hyperintensity is observed in the corpus callosum and the pyramidal tracts, followed by the posterior limb of the internal capsule and the U-shaped fibers. Less hyperintensity is seen in the centrum semiovale. The CSF-filled and gray matter regions appear black. Figure 4 also comprises images of Trace(**D**). A remarkable feature of these images is the absence of contrast variations in the brain parenchyma and the hyperintensity in regions that contain CSF.

Figure 7 shows a diffusion ellipsoid image (axial section) for a region of the brain that includes the splenium of the corpus callosum, the lateral ventricles, and portions of the occipital cortex. The diffusion ellipsoid represents a surface of constant mean-squared displacement of water

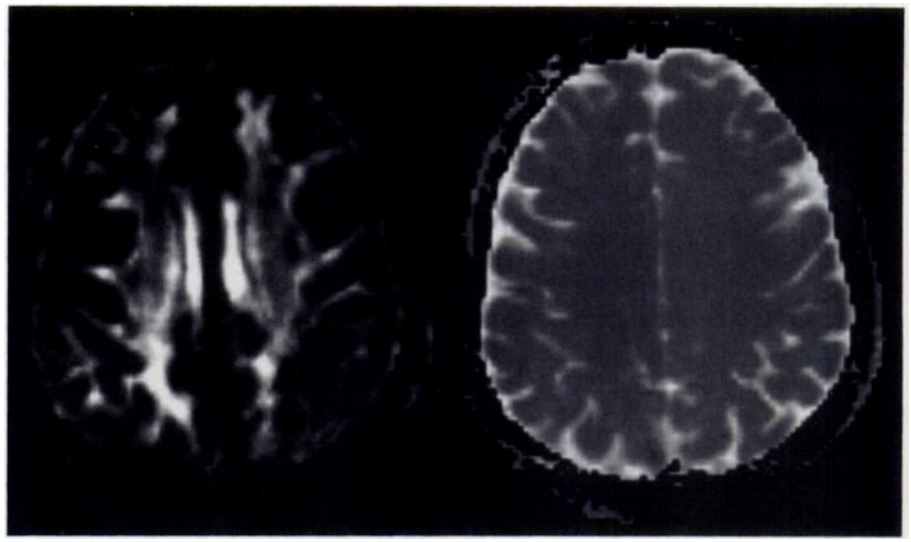

a.

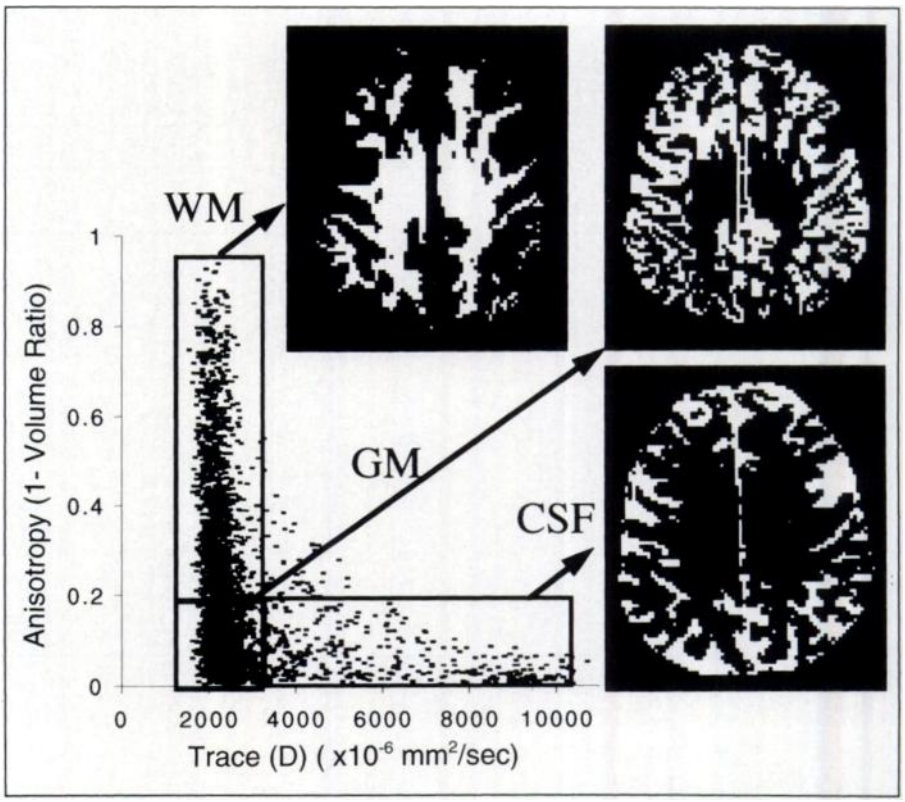

b.

Figure 3. **(a)** Maps of the intravoxel anisotropy index, 1 − Volume Ratio (left) and Trace(**D**) (right). **(b)** Scatter plot of 1 − Volume Ratio versus Trace(**D**) in each voxel. Units of 1 − Volume Ratio are dimensionless. One can identify gray matter, white matter, and CSF regions on the basis of their diffusion properties.

molecules that would arise in a hypothetical experiment in which they were released at the center of the voxel and allowed to diffuse for a time τ. The geometric features of the diffusion ellipsoid are influenced by the physicochemical state, the local material properties, and the microstructure of the tissue. In particular, the diffusion ellipsoid embodies local, intrinsic features of diffusion, such as the degree of anisotropy, and the mean diffusivity, which are extensively treated in this article. Moreover, it displays intrinsic vectorial information about diffusion, in particular, the three principal directions, which include the fiber-tract direction that is depicted by the longest semimajor axis. The striking orientational pattern of prolate ellipsoids in voxels containing the corpus callosum corresponds

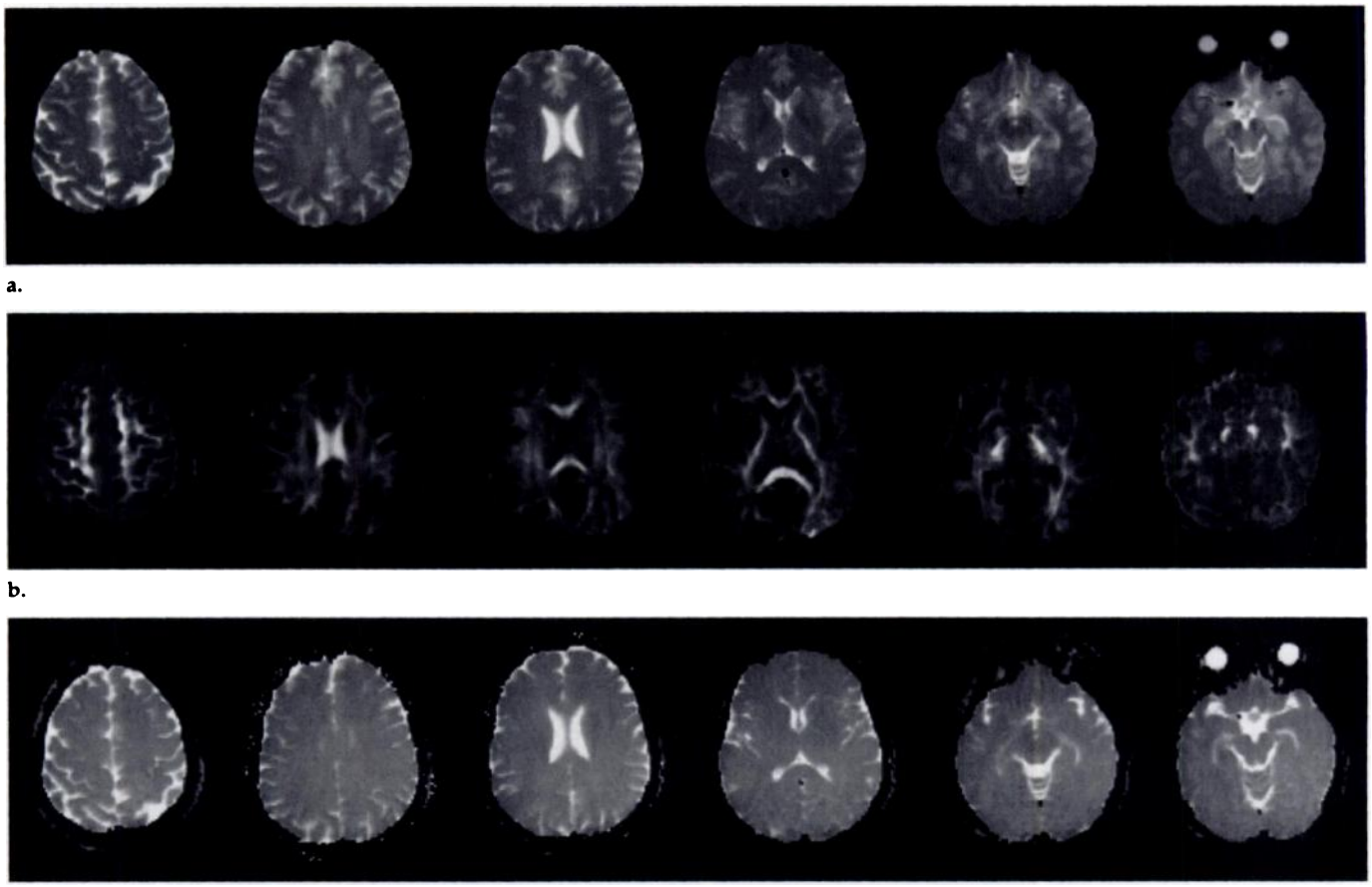

Figure 4. Axial maps of **(a)** the T2-weighted amplitude, **(b)** the (Lattice) anisotropy index, and **(c)** Trace(**D**) in a 33-year-old healthy woman. Anisotropy index images clearly show anisotropic white matter regions as hyperintense and isotropic CSF and gray matter as hypointense. However, the degree of anisotropy varies widely among white matter regions, with higher intensity observed in regions where the fiber pattern is more coherent and lower intensity where it is more incoherent. Note that iron-rich regions, such as the pallidum, the substantia nigra, and the red nucleus, which all appear hypointense in **a**, appear dark in **b**, which permits identification of the neighboring pyramidal tract. **c** clearly shows CSF regions as hyperintense and tissue (gray and white matter regions) as hypointense.

to the expected orientation of the white matter fiber tract in this region.

DISCUSSION

Before discussing the relevance of measures of diffusion derived from the diffusion tensor, it is useful to discuss the effect of noise on their determination. Noise in the DW images introduces variability in the distribution of Trace(**D**) but no bias in its mean value (19). However, for the individual sorted eigenvalues, noise in the DW images not only increases their variability, but also introduces a significant bias in their mean values (19). The severity of this bias depends on the degree of overlap in the distributions of the eigenvalues. If we were to use standard statistical tests, such as analysis of variance, to analyze their distributions in an ROI, we would erroneously conclude that statistically significant differences exist between λ_1 and λ_2, as well as between λ_2 and λ_3, even in isotropic media in which no differences are expected between them. Moreover, bias introduced by sorting the eigenvalues precludes the use of standard statistical tests to assess whether anisotropic diffusion is cylindrically symmetric or asymmetric within a region of interest. Here, we resorted to Monte Carlo simulations of the MR diffusion tensor imaging experiments to explain the observed distribution of eigenvalues within an ROI. Table 3 summarizes the results of this analysis for different anatomical ROIs.

A particularly irksome aspect of this sorting bias is that it makes measures of diffusion anisotropy which depend on the scheme by which eigenvalues are ordered (eg, the ratio of the largest and smallest eigenvalues, λ_1/λ_3; the eccentricity, $[1 - \{\lambda_3/\lambda_1\}2]^{1/2}$) so susceptible to contamination by noise as to preclude their clinical use (19). The lattice anisotropy index and Volume Ratio that we use here are immune to this sorting bias because their values, as with Trace(**D**), are insensitive to the way one orders the eigenvalues.

Trace(D)

Trace(**D**) is homogeneous in the normal brain parenchyma. Its value lies in a narrow range between $1{,}950 \times 10^{-6}$ mm^2/sec and $2{,}200 \times 10^{-6}$ mm^2/sec in most brain regions, which corresponds to an average diffusivity of about 700×10^{-6} mm^2/sec. Only in the cortex is the value of Trace(**D**) ($2{,}477 \times 10^{-6}$ mm^2/sec) significantly different from that in the other anatomic regions we investigated. However, it is likely that this discrepancy is caused by partial volume contamination of CSF in the cortical ROI.

The fact that white matter and gray matter have virtually identical values of Trace(**D**) has no obvious biological explanation at the present time and is worthy of further study. It is also interesting that, in comparing these values of Trace(**D**) with previously acquired values in normal cynomolgus monkeys (19) and cats (36) under similar experimental conditions, we see that its interspecies variability is remarkably low.

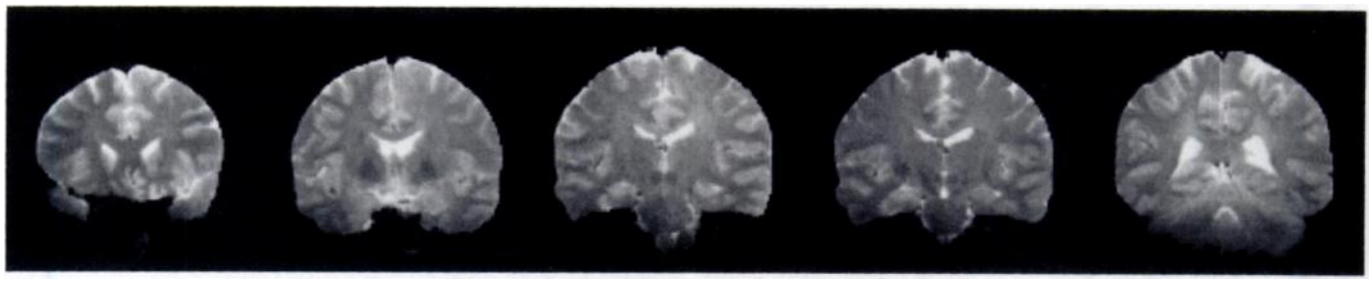

a.

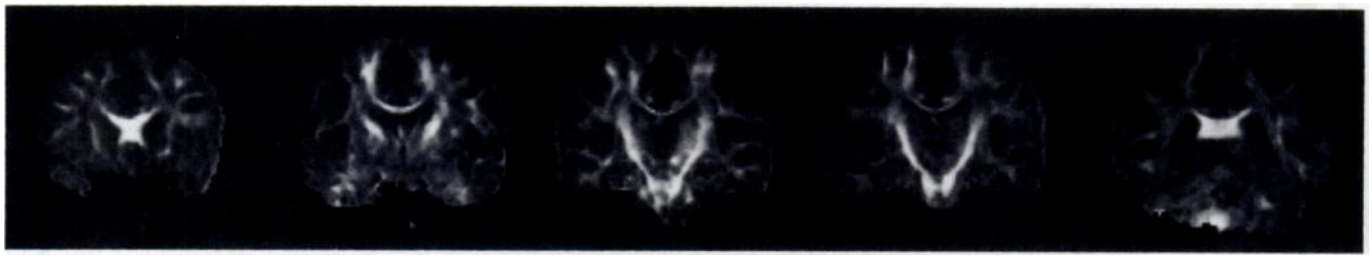

b.

Figure 5. Coronal maps of **(a)** the T2-weighted amplitude and **(b)** the (Lattice) anisotropy index in a healthy 31-year-old woman.

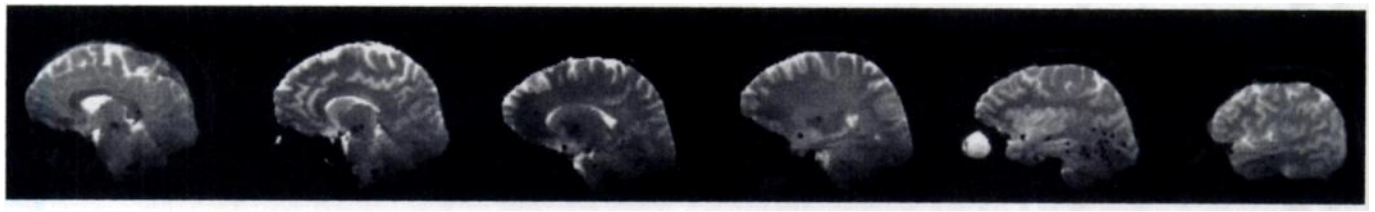

a.

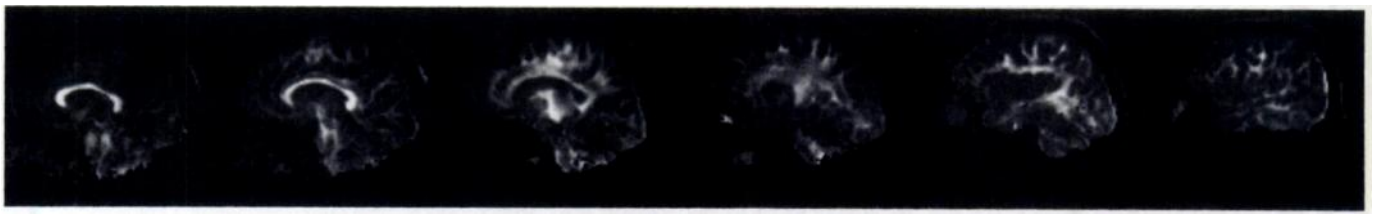

b.

Figure 6. Sagittal maps of **(a)** the T2-weighted amplitude and **(b)** the (Lattice) anisotropy index in a healthy 34-year-old man. Note the high degree of anisotropy in the corpus callosum and the lower degree of anisotropy in many other white matter regions. Some portions of the centrum semiovale are almost isotropic.

Trace(**D**) is independent of the position and orientation of the patient within the magnet, intrinsically has a lower background noise level than an individual ADC, and is unbiased. Moreover, one observes a high degree of uniformity throughout normal brain parenchyma within the same subject, as well as low variability between the brains of different age-matched normal human subjects. These factors make Trace(**D**) a particularly desirable diagnostic parameter since small deviations from its normal value are statistically significant. Consequently, Trace(**D**) may be able to detect more subtle changes in diffusivity (which may occur in degenerative diseases, aging, and development) than the gross changes observed in ischemia. Moreover, its low intersubject variability can potentially improve the quality of pooled data collected in multicenter studies.

It should be noted that although Trace(**D**) is homogeneous in normal brain, its changes in white and gray matter could be different for the same noxious stimulus. For example, the decrease of Trace(**D**) was shown recently to exhibit a different time course in white and gray matter in hyperacute global brain ischemia in cats (36).

Anisotropy

In contrast with Trace(**D**), white matter anisotropy is highly heterogeneous in normal brain parenchyma. We found statistically significant differences in the degree of anisotropy not only between gray matter and white matter regions, but also between almost all white matter regions. In some white matter regions, such as in the corpus callosum and the pyramidal tract, water diffusivity in the direction parallel to the fibers ($\approx 1{,}700 \times 10^{-6}$ mm^2/sec) is approximately seven times larger than the average diffusivity in the perpendicular direction ($\approx 250 \times 10^{-6}$ mm^2/sec). This ratio is much higher than has been reported in all previous studies of diffusion anisotropy in any region of the human brain (15–18). Because the distributions of λ_1 and $([\lambda_2 + \lambda_3]/2)$ clearly do not overlap in both the corpus callosum and the pyramidal tract, their mean values will not be biased in these ROIs. Therefore, the high measured anisotropy is not an artifact caused by the sorting bias mentioned above.

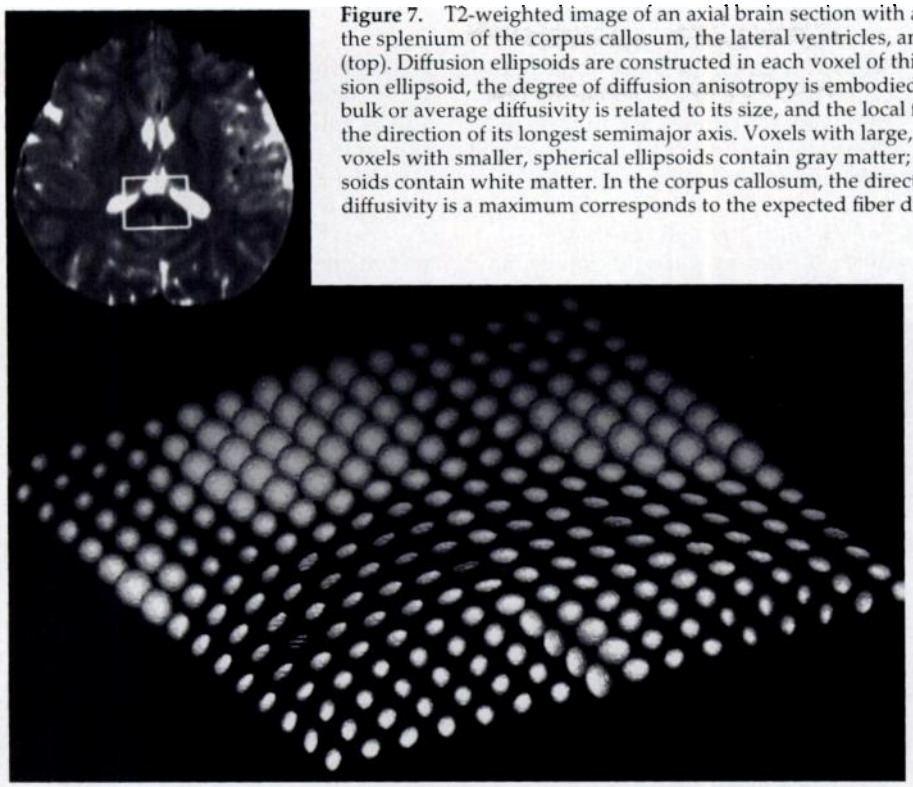

Figure 7. T2-weighted image of an axial brain section with a rectangular ROI that includes the splenium of the corpus callosum, the lateral ventricles, and portions of the occipital cortex (top). Diffusion ellipsoids are constructed in each voxel of this ROI (bottom). For each diffusion ellipsoid, the degree of diffusion anisotropy is embodied in its shape (eccentricity), the bulk or average diffusivity is related to its size, and the local fiber tract direction is given by the direction of its longest semimajor axis. Voxels with large, spherical ellipsoids contain CSF; voxels with smaller, spherical ellipsoids contain gray matter; while voxels with prolate ellipsoids contain white matter. In the corpus callosum, the direction along which the apparent diffusivity is a maximum corresponds to the expected fiber direction in this region.

Table 3
Symmetry of Diffusion in Different Anatomical Structures

ROI	Spherically Symmetric (Isotropic) Diffusion	Cylindrically Symmetric Anisotropic Diffusion	Asymmetric Anisotropic Diffusion
Frontal cortex	Yes		
Caudate nucleus	Yes		
Centrum semiovale			Yes
U fibers			Yes
Optic radiation			Yes
Internal capsule			Yes
Pyramidal tract		Yes	
Corpus callosum		Yes	

We attribute the disparity between our results and those of other studies to the fact that in previous works diffusion anisotropy was calculated from ADCs acquired in two or three perpendicular directions rather than from quantities derived from the diffusion tensor. Ratios of perpendicular ADCs depend on the subject's orientation in the magnet and generally result in underestimation of the degree of anisotropy. To demonstrate the severity of these artifacts, one can form the ratio of the average of the largest and smallest ADCs in the ROI. Using the same data set, we obtained values of ADC_{max}/ADC_{min} of 4.3 and 3.3 in the pyramidal tract and in the corpus callosum, respectively. These resulting anisotropy ratios are consistent with those in previous reports but are still smaller by a factor of two than $\lambda_1/([\lambda_2 + \lambda_3]/2)$.

Nevertheless, the question must be addressed as to how one can explain the high variability in the measurements of diffusion anisotropy observed in the living brain, as well as the low degree of anisotropy seen in some white matter regions. Although the diffusion distances of water (for the given diffusion time in these experiments) are on the order of micrometers, the echo magnitude measured in each voxel reflects an average over a particular voxel. For our voxel size of 9 μL, each voxel contains approximately 10^{20} hydrogen nuclei and, in white matter, approximately 10^6 fibers. Therefore, our diffusion measurement is influenced by molecular, ultrastructural, microstructural, and macrostructural (architectural) features of the tissue.

White matter microstructure.—In particular, the microscopic structure of fibers is likely to affect the measured diffusion anisotropy. Regional differences in fiber packing density, degree of myelination, fiber diameter, and packing density of neuroglial cells could all contribute to the observed variation in diffusion anisotropy. Unfortunately, it is presently difficult to assess their relative effect on the measured voxel-averaged diffusion anisotropy. In white matter, one does not observe regions in which there is a predominance of fibers with only one diameter; rather, one sees a broad distribution of fiber diameters within a voxel. For example, the pyramidal tract contains white matter fibers whose diameter reaches 25 μm (37); however, the majority of fibers are less than 1 μm in diameter.

One might suppose that the packing density of fibers would contribute to the measured diffusion anisotropy. Hajnal et al (8) reported that the packing density of fibers varies tenfold between major tracts and suggested that white matter tracts with a lower packing density could also have a lower anisotropy. The packing density of the fibers is highly variable between different white matter regions: It is reported to be 60,000–70,000/mm^2 in the pyramidal tract (38) and 338,000/mm^2 in the corpus callosum (39). Despite this disparity in the packing density of the fibers, we found no significant difference in the values of anisotropy between these two structures.

One might suppose that diffusion anisotropy is influenced by the packing density of neuroglial cells. However, this quantity is reported to be fairly uniform throughout the brain in both white matter and gray matter (40), so it does not seem to be responsible for the high variability of anisotropy. Moreover, Friede (41) reports that the density distribution of neuroglial cells is slightly lower in the internal capsule and in the pyramidal tract at the level of the cerebral peduncles (37,000–48,000 cells/mm^2) than in the corpus callosum and the optic radiation (85,000 and 96,000 cells/mm^2). Our data in the pyramidal tract and corpus callosum show a similar de-

gree of anisotropy, which is higher than that of the internal capsule and the optic radiation.

One can also speculate that myelin density and distribution are important in determining diffusion anisotropy. Findings of classical ultrastructural studies on myelin in brain white matter suggest that many white matter structures contain a mix of myelinated and nonmyelinated fibers. However, the average amount of myelin in white matter is relatively constant throughout the brain (42). Therefore, it seems that the differences in diffusion anisotropy that we observed in white matter could not be explained by a different degree of myelination in the different structures.

In summary, we were unable to identify a single microstructural factor or a combination of them to account for the observed differences in diffusion anisotropy in all regions of white matter in the normal human brain.

White matter fiber architectural paradigms.—On a grosser length scale, groups of fibers are arranged to form fasciculi or laminae that lie in different planes, run in different directions, and intersect each other in a number of regions. Our diffusion anisotropy data can be explained more consistently by considering these larger-scale architectural patterns of the white matter.

If we could neglect or nullify the effect of noise on the distribution of the eigenvalues of **D**, then the relative magnitudes of the three eigenvalues within each voxel would be sufficient to characterize white matter fiber architecture. Several architectural paradigms are suggested. Each fiber pattern corresponds to a distinct shape of the corresponding diffusion ellipsoid.

$\lambda_1 \approx \lambda_2 \approx \lambda_3$.—This is the typical distribution of the eigenvalues that we would expect in a medium in which diffusion is isotropic at a microscopic level, as in free water. We must consider, however, that apparent isotropy could result from structures that are anisotropic at the microscopic level but that are randomly oriented within the voxel. In white matter, this could occur where fibers cross in a spherically symmetric pattern. On our images, this pattern is evident in some regions of the centrum semiovale at the intersection of fibers of the radiation of the corpus callosum, association fibers, and fibers of the corona radiata.

$\lambda_1 \gg \lambda_2 \approx \lambda_3$.—This configuration corresponds to a cigar-shaped diffusion ellipsoid that is cylindrically symmetric. This distribution of eigenvalues is consistent with the arrangement of white matter fibers in parallel bundles with their longitudinal axis aligned with ε_1, the eigenvector associated with λ_1. In the anatomic regions that we have considered in this study, this pattern is found in the pyramidal tract and in the corpus callosum.

$\lambda_1 \approx \lambda_2 \gg \lambda_3$.—This configuration corresponds to a cylindrically symmetric diffusion ellipsoid that is pancake- or pizza-shaped. This distribution of eigenvalues is consistent with white matter fibers that have their longitudinal axes oriented either orthogonally or randomly in the plane that contains ε_1 and ε_2 (where ε_2 is the eigenvector associated with λ_2). Fibers could be regularly oriented within sheets, but those sheets could themselves be stacked within a voxel so that the voxel-averaged orientation appears random in the ε_1-ε_2 plane. This pattern is not highly represented in the brain. We found it in peripheral regions of the centrum semiovale, especially at the intersection of long association fibers with fibers of the corona radiata.

$\lambda_1 > \lambda_2 > \lambda_3$.—This configuration corresponds to an asymmetric diffusion ellipsoid whose semimajor axes are all unequal. In general, this suggests the presence of fibers that run in multiple directions within the voxel but that maintain, on average, a preferential direction. It could represent intermediate stages between the cigar and pancake configurations, depending on the relative magnitude of each eigenvalue. This is the pattern represented in the majority of voxels in the white matter of the brain. Given the complicated direction field of white matter fibers in the brain, this is not surprising. The degree of asymmetry is variable in different regions. For instance, the posterior limb of the internal capsule and the optic radiation do not exhibit cylindrical symmetry (see Table 3), but their degree of asymmetry is lower than that of the U fibers and the centrum semiovale.

Experimental Design Issues in Diffusion Tensor MR Imaging

Many technical obstacles have impeded the widespread implementation of diffusion imaging and diffusion tensor imaging in the clinic. These include a dearth of gradient coils capable of producing sufficiently strong magnetic field gradient pulses to produce diffusion sensitization, the absence of fast imaging sequences that produce high-quality DW images, and the difficulty in controlling for motion artifacts.

Gradient calibration and b-matrix computation.—Errors in the estimated diffusion tensor can originate from gradient miscalibration, miscalculation of the b-matrix, or both. The effect of imaging gradients on the b-matrix has been extensively described previously (30) and will not be discussed here. Our experience suggests that with imaging parameters typical of a clinical study, if the imaging gradients are refocused immediately after they are applied, their contribution to the b-matrix, and thus the echo attenuation, is minimal. If the sequence is not optimally designed, however, the contributions of imaging gradients (cross terms) can be treated in the estimation of **D**.

Number of sampling directions.—To estimate the entire diffusion tensor, one must apply diffusion gradients along at least six noncollinear directions (20). Typically, this is achieved by applying different combinations of x, y, and z diffusion gradient pulses simultaneously. Because one generally does not know the distribution of fiber directions in the tissue a priori, it is prudent to sample these gradient directions uniformly. However, hardware limitations introduce constraints on the maximum gradient amplitude one can apply and thus on the maximum diffusion attenuation achievable in a DW image. In most cases, the surface along which the diffusion gradient vector has a maximum length is a cube. To maximize the S/N per unit time in a DW image, one should apply gradients that point to the vertices of this cube (43). However, this sampling strategy yields only four independent gradient directions, while six are required to adequately describe diffusion anisotropy in all white matter regions.

The methods proposed by Conturo et al (43) and Hsu and Mori (44) are in principle appropriate for characterization of anisotropy in regions of the normal brain, such as the pyramidal tract and the corpus callosum, where cylindrical symmetry of diffusion is verified. We do not know, however, if these regions will still exhibit cylindrical symmetry in pathologic conditions.

Here, we decided to sample six gradient directions isotropically by applying combinations of diffusion gradient pairs. Even more efficient gradient configurations that still maintain an isotropic sampling pattern can be achieved by increasing the number of gradient directions.

Recently, isotropically weighted sequences have been proposed (45, 46). These produce DW images whose contrast is proportional to Trace(**D**)

by effectively applying multiple gradients with different directions within the same sequence. This interesting acquisition scheme, however, has an intrinsically low S/N per unit time as compared with a multiple-direction sampling pattern and provides no information about diffusion anisotropy.

Number of diffusion increments for each direction.—In brain tissue, where there is a large range in the observed principal diffusivities (eigenvalues), it is prudent to obtain DW images with a range of b-matrix values. A good rule of thumb to ensure that the variance of the estimated principal diffusivity, λ_i, is acceptably low is to see that its b value is approximately equal to $1/\lambda_i$. It is easy to see that b values of 300–400 sec/mm^2 obtained with conventional gradients (10 mT/m) are much lower than the $1/\lambda_2$ and $1/\lambda_3$ we measured in some white matter fiber tracts and thus are too small to provide adequate estimates of the diffusivity perpendicular to the fibers. Errors in the estimation of the diffusivity perpendicular to the fibers have little effect on the value of Trace(**D**) but can substantially affect accuracy and the precision of the measurements of anisotropy. Therefore, in clinical MR systems equipped with low-power gradients, a reliable assessment of anisotropy may be difficult to attain.

Voxel-by-voxel computation versus signal intensity averaging within a ROI.—If one wishes to characterize diffusion adequately in a heterogeneous, anisotropic medium such as the human brain, it is necessary first to determine diffusion parameters derived from **D** (eigenvalues, anisotropy indices, etc) within each voxel and then to average them within an anatomic ROI rather than first to average the signal intensity within the entire ROI and then calculate the diffusion parameters of interest. Signal intensity averaging within a ROI, like decreasing image resolution, effectively powder averages the quantities of interest. In particular, measures of diffusion anisotropy will often be reduced by signal intensity averaging within a ROI.

Misregistration caused by eddy currents.—Care should be taken to eliminate not only motion artifacts, but also eddy currents, which tend to cause shearing and dilation in DW images, as described above.

Summary and Clinical Perspective

The acquisition of the entire diffusion tensor allows one to produce maps of distinct intrinsic features of the diffusion process, such as the average diffusivity, diffusion anisotropy, and the principal directions of diffusion. The resulting images are easier to interpret than conventional diffusion images, such as DW images and ADC maps, whose contrast results from a complicated combination of mean diffusion, anisotropy, and fiber direction.

In the normal brain, differences in local fiber architecture and organization are reflected in a highly variable degree of diffusion anisotropy within different white matter regions. For example, diffusion anisotropy is much lower in subcortical regions, where the direction field of fibers is less coherent than it is in the corpus callosum or the pyramidal tract, where fibers are more homogeneously oriented. However, in the latter regions, the degree of diffusion anisotropy is approximately three times higher than what was previously reported. The assumption of cylindrical symmetry of diffusion, which is widely used, also is not supported by experimental findings in many brain white matter regions.

Scalar quantities derived from the diffusion tensor can be used to segment normal brain tissue into CSF, gray matter, and white matter compartments, as well as to classify tissues on the basis of their diffusion properties. Moreover, the rotationally invariant quantities derived from **D**, such as the lattice anisotropy index and Trace(**D**), can be used in conjunction with other intrinsic MR quantities, such as T1 and T2, in multiparametric image analysis.

In summary, diffusion tensor imaging provides a quantitative and informative description of diffusion in anisotropic and heterogeneously oriented media, which is impossible to achieve by using DW images or ADCs acquired in two or three orthogonal directions. However, the acquisition and processing of a diffusion tensor data set requires the estimation of more parameters than does conventional diffusion imaging; therefore, it is intrinsically more time-consuming. So, from a clinical perspective, one must ascertain whether the additional benefits provided by diffusion tensor imaging exceed the additional costs.

Clinical requirements effectively dictate the preferred method to use to measure water diffusion properties in the human brain. If one is interested in determining whether a patient has had an acute ischemic event, DW images acquired with gradients applied in only one direction might suffice. If it is necessary to determine the extent and severity of the infarct, or if it is advisable to perform a follow-up study of acute ischemia, we recommend determining Trace(**D**), perhaps by using the method proposed by Conturo and colleagues (43), who applied a direction pattern of the diffusion gradients that is especially efficient in terms of S/N per unit time. However, if one is interested in performing quantitative studies in which diffusion anisotropy could also be informative, we recommend acquiring the entire diffusion tensor. This would apply to long-term studies of stroke, where it has already been observed that changes in diffusion anisotropy indicate Wallerian degeneration and gliosis (47), as well as to a variety of other neurologic disorders, which include the assessment of incomplete white matter maturation, demyelination, tumor growth, and degenerative diseases. ■

References

1. Merboldt KD, Hanicke W, Frahm J. Self-diffusion NMR imaging using stimulated echoes. J Magn Reson 1985; 64:479–486.
2. Le Bihan D, Breton E, Lallemand D, Grenier P, Cabanis E, Laval-Jeantet M. MR imaging of intravoxel incoherent motions: application to diffusion and perfusion in neurologic disorders. Radiology 1986; 161: 401–407.
3. Taylor DG, Bushell MC. The spatial mapping of translational diffusion coefficients by the NMR imaging technique. Phys Med Biol 1985; 30:345–349.
4. Le Bihan D, Turner R, Douek P, Patronas N. Diffusion MR imaging: clinical applications. AJR 1992; 159:591–599.
5. Warach S, Chien D, Li W, Ronthal M, Edelman RR. Fast magnetic resonance diffusion-weighted imaging of acute human stroke. Neurology 1992; 42:1717–1723.
6. Moseley ME, Cohen Y, Mintorovitch J, et al. Early detection of regional cerebral ischemia in cats: comparison of diffusion- and T2-weighted MRI and spectroscopy. Magn Reson Med 1990; 14:330–346.
7. Doran M, Hajnal JV, Van Bruggen N, King MD, Young IR, Bydder GM. Normal and abnormal white matter tracts shown by MR imaging using directional diffusion weighted sequences. J Comput Assist Tomogr 1990; 14:865–873.
8. Hajnal JV, Doran M, Hall AS. MR imaging of anisotropically restricted diffusion of water in the nervous system: technical, anatomic, and pathologic considerations. J Comput Assist Tomogr 1991; 15:1–18.
9. Moseley ME, Cohen Y, Kucharczyk J, et al. Diffusion-weighted MR imaging of anisotropic water diffusion in cat central nervous system. Radiology 1990; 176:439–445.
10. Cleveland GG, Chang DC, Hazlewood CF, Rorschach HE. Nuclear magnetic resonance measurement of skeletal muscle: anisotropy of the diffusion coefficient of the intracellular water. Biophys J 1976; 16:1043–1053.
11. Reese TG, Weisskoff RM, Smith RN, Rosen R, Dinsmore RE, van Wedeen J. Imaging myocardial fiber architecture in vivo with magnetic resonance. Magn Reson Med 1995; 34:786–791.

12. Yang Y, Shimony JS, Xu S, Gulani V, Dawson MJ, Lauterbur PC. A sequence for measurement of anisotropic diffusion by projection reconstruction imaging and its application to skeletal and smooth muscle (abstr). In: Proceedings of the Society of Magnetic Resonance 1994. Berkeley, Calif: Society of Magnetic Resonance, 1994; 1036.
13. Muller MF, Prasad PV, Bimmler D, Kaiser A, Edelman RR. Functional imaging of the kidney by means of measurement of the apparent diffusion coefficient. Radiology 1994; 193:711–715.
14. Wu JC, Wong EC, Arrindell EL, Simons KB, Jesmanowicz A, Hyde JS. In vivo determination of the anisotropic diffusion of water and the T1 and T2 times in the rabbit lens by high-resolution magnetic resonance imaging. Invest Ophthalmol Vis Sci 1993; 34: 2151–2158.
15. Sakuma H, Nomura Y, Takeda K, et al. Adult and neonatal human brain: diffusional anisotropy and myelination with diffusion-weighted MR imaging. Radiology 1991; 180:229–233.
16. Le Bihan D, Turner R, Douek P. Is water diffusion restricted in human brain white matter? An echo-planar NMR imaging study. Neuroreport 1993; 4:887–890.
17. Nomura Y, Sakuma H, Takeda K, Tagami T, Okuda Y, Nakagawa T. Diffusional anisotropy of the human brain assessed with diffusion-weighted MR: relation with normal brain development and aging. AJNR 1994; 15:231–238.
18. Brunberg JA, Chenevert TL, McKeever PE, et al. In vivo MR determination of water diffusion coefficients and diffusion anisotropy: correlation with structural alteration in gliomas of the cerebral hemispheres. AJNR 1995; 16:361–371.
19. Pierpaoli C, Basser PJ. Toward a quantitative assessment of diffusion anisotropy. Magn Reson Med 1996; 36:893–906.
20. Basser PJ, Mattiello J, LeBihan D. Estimation of the effective self-diffusion tensor from the NMR spin echo. J Magn Reson B 1994; 103:247–254.
21. Basser PJ, Mattiello J, LeBihan D. MR diffusion tensor spectroscopy and imaging. Biophys J 1994; 66:259–267.
22. Le Bihan D. Diffusion and perfusion magnetic resonance imaging. New York, NY: Raven, 1995.
23. Jezzard P, Pierpaoli C. Diffusion mapping using interleaved spin echo and STEAM EPI with navigator echo correction (abstr). In: Proceedings of the Society of Magnetic Resonance 1995. Berkeley, Calif: Society of Magnetic Resonance, 1995; 903.
24. Asato R, Tsukamoto T, Okumura R, Miki Y, Yoshitome E, Konishi J. A navigator echo technique effectively eliminates phase shift artifacts from the diffusion weighted head images obtained on the conventional NMR imager (abstr). In: Book of abstracts: Society of Magnetic Resonance in Medicine 1992. Berkeley, Calif: Society of Magnetic Resonance in Medicine, 1992; 1226.
25. Ordidge RJ, Helpern JA, Qing ZX, Knight RA, Nagesh V. Correction of motional artifacts in diffusion-weighted MR images using navigator echoes. Magn Reson Imaging 1994; 12:455–460.
26. Anderson AW, Gore JC. Analysis and correction of motion artifacts in diffusion weighted imaging. Magn Reson Med 1994; 32:379–387.
27. de Crespigny AJ, Marks MP, Enzmann DR, Moseley ME. Navigated diffusion imaging of normal and ischemic human brain. Magn Reson Med 1995; 33:720–728.
28. Marks MP, de Crespigny A, Lentz D, Enzmann DR, Albers GV, Moseley ME. Acute and chronic stroke: navigated spin-echo diffusion-weighted MR imaging. Radiology 1996; 199:403–408.
29. Stejskal EO, Tanner JE. Spin diffusion measurements: spin echoes in the presence of time-dependent field gradient. J Chem Phys 1965; 42:288–292.
30. Mattiello J, Basser PJ, LeBihan D. Analytical expression for the b matrix in NMR diffusion imaging and spectroscopy. J Magn Reson 1994; 108:131–141.
31. Henkelman RM. Measurement of signal intensities in the presence of noise in MR images. Med Phys 1985; 12:232–233.
32. Bevington PR. Data reduction and error analysis for the physical sciences. New York, NY: McGraw-Hill, 1969.
33. Press WH. Eigensystems. In: Numerical recipes in C: the art of scientific computing. 2nd ed. New York, NY: Cambridge University Press, 1992; 478–481.
34. Pierpaoli C, Mattiello J, Le Bihan D, Di Chiro G, Basser PJ. Diffusion tensor imaging of brain white matter anisotropy (abstr). In: Proceedings of the Society of Magnetic Resonance 1994. Berkeley, Calif: Society of Magnetic Resonance 1994; 1038.
35. Pierpaoli C, Basser PJ. New invariant "lattice" index achieves significant noise reduction in measuring diffusion anisotropy (abstr). In: Proceedings of the International Society of Magnetic Resonance in Medicine 1996. Berkeley, Calif: International Society of Magnetic Resonance in Medicine, 1996; 1326.
36. Pierpaoli C, Baratti C, Jezzard P. Fast tensor imaging of water diffusion changes in gray and white matter following cardiac arrest in cats (abstr). In: Proceedings of the International Society of Magnetic Resonance in Medicine 1996. Berkeley, Calif: International Society of Magnetic Resonance in Medicine, 1996; 314.
37. Blinkov S, Glezer I. The human brain in figures and tables. New York, NY: Plenum, 1968.
38. Weil A, Lassek A. The quantitative distribution of the pyramidal tract in man. Arch Neurol Psychiatry 1929; 22:495–510.
39. Tomasch J. A quantitative analysis of the human anterior commissure. Acta Anat 1957; 30:902–906.
40. Blinkov S, Ivanitskii G. The number of glial cells in the human brain: computer calculation. Biofizika 1965; 10:817–825.
41. Friede R. A histochemical study of diaphorase in human white matter with some notes on myelination. J Neurochem 1961; 17–30.
42. Yakovlev P, Lecours A. The myelogenetic cycles of regional maturation of the brain. Philadelphia, Pa: Davis, 1967.
43. Conturo TE, McKinstry RC, Akbudak E, Robinson BH. Encoding of anisotropic diffusion with tetrahedral gradients: a general mathematical diffusion formalism and experimental results. Magn Reson Med 1996; 35:399–412.
44. Hsu EW, Mori S. Analytical expressions for the NMR apparent diffusion coefficients in an anisotropic system and a simplified method for determining fiber orientation. Magn Reson Med 1995; 34:194–200.
45. Wong EC, Cox RW, Song AW. Optimized isotropic diffusion weighting. Magn Reson Med 1995; 34:139–149.
46. Mori S, van Zijl PCM. Diffusion weighting by the trace of the diffusion tensor with a single scan. Magn Reson Med 1995; 33: 41–52.
47. Pierpaoli C, Barnett A, Penix L, De Graba T, Basser PJ, Di Chiro G. Identification of fiber degeneration and organized gliosis in stroke patients by diffusion tensor MRI (abstr). In: Proceedings of the International Society of Magnetic Resonance in Medicine 1996. Berkeley, Calif: International Society of Magnetic Resonance in Medicine, 1996; 563.